A Hybrid Fault Cluster and Thévenin Equivalent Based Framework for Rotor Angle Stability Prediction

Seyed Mahdi Mazhari, *Member, IEEE*, Nima Safari, *Student Member, IEEE*, C.Y. Chung, *Fellow, IEEE*, and Innocent Kamwa, *Fellow, IEEE*

***Abstract*—This paper addresses a novel approach for rotor angle stability prediction in power systems. In the proposed framework, a fault cluster (FC) concept is introduced to divide an electrical network into several disparate zones. FCs are determined in accordance with the installed PMU locations so that the well-developed wide-area fault detection modules can estimate the origin of any fault in the network among FCs. The proposed framework assigns a stability prediction model to each FC. Parameters of the Thévenin equivalent network (TEN) seen from some generators are calculated both in steady-state and during fault; the TEN parameters are then applied as inputs to the prediction models. The proposed method benefits from parallel computation in the training process and does not require post-fault data. The performance of the proposed distributed framework is validated on several IEEE test systems, followed by a discussion of results.**

***Index Terms*—Decision tree, fault cluster (FC), feature selection, phasor measurement unit (PMU), Thévenin equivalent, transient stability.**

I. Introduction

POWER systems are usually confronted with various weather conditions and fortuitous events that may lead to incidents causing partial or complete instability of the network. Transient stability refers to the ability of the system to maintain synchronism of generators and bring itself back to a stable steady-state following a large disturbance [1]. Transient instability is among the most infrequent, yet most severe, events in power systems and can bring about unintended islanding, cascading outages, and widespread blackouts.

Conventionally, power system operating limits are conservatively set to prevent system instability; therefore, optimal exploitation of the existing facilities is confined [2]. However, rapid development of phasor measurement units (PMUs), as part of the wide-area measurement system, paved the way for network operation closer to stability limits. Early prediction of rotor angle stability based on PMU data can trigger sets of emergency control strategies that can prevent or reduce destructive impacts of large disturbances [3].

Several methods and algorithms have been developed for rotor angle stability prediction in recent years. Time-domain analysis of an identified event with respect to the system parameters is the most conventional and accurate approach to tackle this problem [4], [5]; however, unaffordable computational burden hinders its application to online prediction [6]. Transient-energy-function based algorithms form another group of techniques in which variations of kinetic and potential energies against reference values are employed as criteria for stability assessment [7], [8]. Nonetheless, calculating levels of these energies following certain contingencies is challenging in real-life power systems [9].

Data-driven approaches offer an alternative framework for online stability prediction; these methods engage sophisticated artificial intelligence (AI) techniques to find a prediction model over a large set of training data obtained by offline analysis. Notably, data-driven based algorithms (DDA) have garnered interest in recent years due to their advantages in real-time applications [10]–[17]. Various techniques have been developed based on this approach for either pre- or post-fault system variables. In [10], post-fault rotor angles of generators are preprocessed and then fed into a hybrid classifier composed of probabilistic neural networks (NNs). Application of adaptive artificial NNs is also investigated in [11] in which a pre-disturbance operating point is employed to predict system stability. Performance of a support vector machine is evaluated in [12], [13]; in both papers, post-fault rotor angles are used as inputs to the prediction model, though [12] also uses generator speeds and voltages in the training process. Significant success with robustness of decision tree (DT) [13]–[15], core vector machine [16], and extreme learning machine [17] have been reported; furthermore, new indices have been introduced for feature extraction in [14], [15] and a feature selection process employed by [16] and applied to a wide array of pre- and post-disturbance parameters in the specialized literature.

To date, the majority of AI-based algorithms for stability prediction have been formed based on post-fault or pre-disturbance information [9]–[17]. However, PMU devices benefit from high sampling rates and can provide useful data during a fault, even though it is very short [18]. Recent publications use the first few cycles of post-disturbance data (~2 cycles), which is less than the duration of a large proportion of faults observed in real-life systems [9], [17]. Thus, performance of the data extracted from synchronized measurement devices during disturbances can be evaluated with more focus.

Moreover, the structure of DDAs to address the current problem has remained largely unchanged in recent years; therefore, several recent advancements in PMU-related studies can now be included in the stability prediction problem. Amongst them, fault

Manuscript sent September 15, 2017. This work was supported in part by the Natural Sciences and Engineering Research Council (NSERC) of Canada and the Saskatchewan Power Corporation (SaskPower).

S.M. Mazhari, N. Safari, and C.Y. Chung are with the Department of Electrical and Computer Engineering, University of Saskatchewan, Saskatoon S7N 5A9, Canada(e-mail: s.m.mazhari@usask.ca; n.safari@usask.ca; c.y.chung@usask.ca).

I. Kamwa is with the Hydro-Québec/IREQ, Power System and Mathematics Varennes QC J3X 1S1, Canada (e-mail: kamwa.innocent@ireq.ca)

location detection and fault area estimation are introduced in [18]–[20] and online event and fault type detection are reported in [21], [22]. These methods realize a reliable estimate of fault area, fault type, and fault duration, which are determinative factors in system instability. Moreover, some state-of-the-art algorithms can determine real-time parameters of the Thévenin equivalent network (TEN) seen from different buses by means of PMU measurements [23]–[25]. The TEN is widely used in various power system analysis problems; however, its efficacy in DDA-based stability prediction requires further investigation.

Although past methods conduct offline simulations in parallel to shape the database, the overall training process does not benefit from parallel computation because the training process begins once the whole database is constructed. Such deficiency may either confine application of some AI-based methods or curb the generation of more training data in large-scale networks [26].

In addition, considering the importance of quick action against instability, several methods have been introduced in recent years to try and reduce the amount of post-fault data required for faster prediction of stability status [9], [17]. Thus, approaches that can predict stability without post-fault data not only decrease response time to the lowest possible value but can also be used in conjunction with [9]–[17] to increase the performance of and confidence in the prediction process.

Aimed at addressing the above-mentioned shortcomings of the prediction approaches proposed to date, and benefiting from advancements in PMU-related studies, a novel framework is put forward. A fault cluster (FC) concept is developed in which a typical network is divided into several areas to ensure performance of the prevalent fault area estimation and fault detection algorithms with respect to the PMU layout. A new feature extraction approach is employed in which parameters of the TEN seen from generators are calculated both in steady-state and during fault. A feature selection algorithm is also employed to minimize the required amount of input data and subsequently increase the robustness of the proposed method against PMU losses. The developed approach finds a prediction model for each FC, solely relying on a portion of training data dedicated to faults occurring in that area. Thus, it takes advantage of parallel processing in the training stage. Finally, the effectiveness of the developed framework is assessed and compared with existing approaches using several IEEE test systems, including 10-, 16-, 48-, and 50-machine networks.

II. Methodology

As noted above, outcomes of recent studies on PMU applications are used in this paper to form a novel stability predication framework. Explanations and justifications for the adaptability of such approaches to the current problem are described in this section.

A. PMU-Based Fault Location Estimation

Once a fault occurs in a power system, voltages measured at buses near the fault location observe the largest changes in comparison to other parts of the network. PMU data can be used to

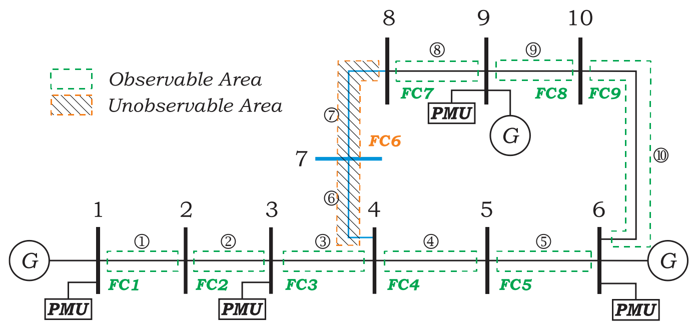

Fig. 1. FCs in a network with PMUs located on buses 1, 3, 6, and 9.

find exact fault locations in a fully-observable network [27]. However, considering line outages, PMU failures, and unavailability of PMUs at every bus of the network, precise fault locating may not always be possible. In these cases, fault region identification can be calculated with a limited number of PMUs [18]–[20]. The authors of [18] introduced an algorithm in which the suspicious fault region is computed with 100% accuracy. In [19], a travelling wave-based method is employed to estimate fault areas while PMUs are distributed based on a given limited depth-of-unobservability (DOU) [27], [28]. Finally, [20] addresses a fault estimation method in which PMUs are only installed in generation buses.

B. The Proposed Fault Cluster (FC) Concept

Based on the explanations in the previous section, recent advancements have made it feasible to obtain a reliable estimate of the fault area even with a limited number of PMUs. At least two PMUs should be installed in an interconnected network for fault area detection purposes [18]; as the number of PMUs in a network increases, fault detection can be accomplished with more accuracy. Based on information about the fault area, stability prediction of a bulk power system can be conducted by zeroing in on the analysis of the suspicious FC. This approach not only omits a huge amount of irrelevant data used in the prediction phase, but also markedly enhances the accuracy and speed of the estimator and facilitates distributed computing in the training process.

The main reasoning behind the FC concept is to divide an electrical system into several disparate areas, called FCs. In this way, the prevalent wide-area fault detection methods can determine the fault location among FCs [18]–[20], [27].

Fig. 1. represents an illustrative example in which a 10–bus network is reinforced by four PMUs. PMUs are distributed so that bus 7 remained unobservable. In this case, a fault occurring in lines that are connected to that bus but may not be exactly identified, though the fault area can be recognized with acceptable reliability [18]–[20]. Hence, all lines connected to bus 7 are selected as a single FC. The figure shows that the remaining lines are chosen as independent FCs because buses at both ends of the lines are observable; thus, the 10-bus network is dissected into nine FCs as shown in Fig. 1.

Different from the prior stability prediction methods in which a single model is trained for the whole network, this study trains and assigns a prediction model to each FC; as such, nine different

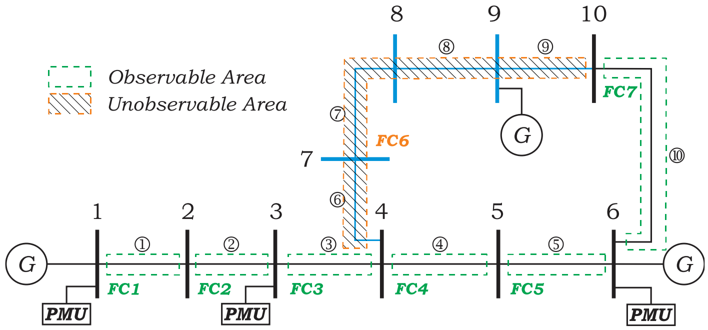

Fig. 2. FCs in a network with PMUs located on buses 1, 3, and 6.

models will be developed for Fig. 1. Because the FCs play a weighty role in the proposed approach, they should be defined so that loss of lines or PMU failures does not affect the fault area estimation [27]. The following steps explain the FC detection method used in this paper.

1) *Receive data*

A set of line and PMU outages (Ω^{O}), set of network lines (Ω^{l}), and set of PMUs (Ω^{p}) are received from the user. Note that $|\Omega^{O}| = |\Omega^{l}| + |\Omega^{p}| + 1$ in order to consider a normal network topology accompanied by all possible single line and PMU outages.

2) *Find observable buses and lines*

For each array of Ω^{O}, such as s, a set of observable buses (Ω_s^{ob}) and observable lines (Ω_s^{ol}) are constructed by (1)–(4):

$$\Omega_s^{ob} = \{\forall\, i \in \Omega^{b} \mid \zeta_i = 1\} \tag{1}$$

$$\Omega_s^{ol} = \left\{\forall\, i \in \Omega^{l} \mid \zeta_k = \zeta_j = 1, (k,j) \in \Omega_i^{b}\right\} \tag{2}$$

$$\zeta_i = \begin{cases} 1 & f_i^{ob} \geq 1 \\ 0 & f_i^{ob} = 0 \end{cases} \qquad \forall\, i \in \Omega^{b} \tag{3}$$

$$f_i^{ob} = \sum_{k \in \Omega_i^{ne}} \beta_k \qquad \forall\, i \in \Omega^{b} \tag{4}$$

where Ω^{b} and Ω_i^{b} are the set of network buses and pair of buses connected to line i, respectively; ζ_i represents a binary decision variable that is equal to 1 if bus i is observable and 0 otherwise; f_i^{ob} is an observability function of bus i; β_k indicates a binary decision variable that is equal to 1 if a PMU is installed at bus i and 0 otherwise; and Ω_i^{ne} stands for a set of neighboring buses of bus i, including itself.

3) *Find initial FCs*

While observable buses and lines are calculated in the previous stage, a set of FCs is defined for each array of Ω^{O}. To this end, each observable line is considered to be a single FC. Then, all observable lines are removed from Ω^{l} to form a new system for further investigation. Afterwards, the first bus of the new system is selected and the depth-first search (DFS) algorithm is conducted to find the interconnected subgraph connected to this bus [29]. The elements of this entire subgraph are considered to be another FC and are removed from Ω^{l}. The DFS is applied to another unobservable bus of the new system and this process continued until $|\Omega^{l}| = 0$.

TABLE I
FCs OBTAINED FOR FIG. 1 UNDER DIFFERENT CONTINGENCIES

Case	Failed PMU	# of FCs	FCs
1	--	9	{①},{②},{③},{④},{⑤},{⑥,⑦},{⑧},{⑨},{⑩}
2	bus 1	9	{①},{②},{③},{④},{⑤},{⑥,⑦},{⑧},{⑨},{⑩}
3	bus 3	6	{①},{②,③,④,⑥,⑦},{⑤},{⑧},{⑨},{⑩}
4	bus 6	7	{①},{②},{③},{④,⑤,⑩},{⑥,⑦},{⑧},{⑨}
5	bus 9	7	{①},{②},{③},{④},{⑤},{⑥,⑦,⑧,⑨},{⑩}
Cases 1–5		12	{①},{②},{③},{④},{⑤},{⑥,⑦},{⑧},{⑨},{⑩},{④,⑤,⑩}, {②,③,④,⑥,⑦},{⑥,⑦,⑧,⑨}

4) *Determine final FCs*

To find the final FCs, the union operator is applied to the initial FCs obtained in the latter stage.

The 10-bus system shown in Figs. 1–2 is employed to provide more information about the overall FC determination algorithm. Two different contingencies are considered: 1) no loss of line or PMU and 2) loss of PMU located at bus 9. For the former case, as illustrated in Fig. 1, bus 7 is unobservable based on the formulation addressed in Step 2. All unobservable buses and lines are shown by hatched area. Lines ①–⑤ and ⑧–⑩ are observable and each will form a single FC. By removing these lines from the network, each connected subgraph with at least one line will be considered as an FC. In this case, one subgraph consisting of lines ⑥ and ⑦ is available. Thus, nine FCs, as shown in Fig. 1, are available for the first case. The network of the second study is shown in Fig. 2. In this case, buses 7–9 are unobservable. Lines ①–⑤ and ⑩ create distinct FCs and a subgraph consisting of lines ⑥–⑨ form a single FC. Hence, seven FCs are available in the latter case, as shown in Fig. 2.

The obtained initial FCs associated with the discussed cases accompanied by those of other PMU outages are summarized in Table I. The table shows that 12 FCs are selected as the final FC layout for this network with respect to PMU failures; this means 12 prediction models will be developed for this network. Note that line outages or other complex contingencies can be considered without loss of generality. Moreover, the FC determination algorithm is solved only once for any network but can be updated in case of network expansions.

C. *Thévenin Equivalent Network (TEN) Calculation*

The Thévenin equivalent represents a compact abstraction and accurate substitute of a network; it is widely used to solve various power system problems in which a portion of the system data is unavailable [24]. With recent advancements in PMU technology, the TEN parameters can be efficiently determined in real-time, especially in cases with considerable changes in power frequency [27]. If the generator dynamics are faster than the grid dynamics, the grid can be replaced by its TEN representing a single voltage source (v_i^{T}) in series with an impedance (z_i^{T}), as shown in Fig. 3. At each instant of time (t), the TEN parameters seen from a generator (i) can be calculated with two consecutive synchronized measurements, as follows [23]:

$$z_i^{T}(t) = \frac{\overline{V_i^{G}}(t+1) - V_i^{G}(t)}{\overline{I_i^{G}}(t+1) - I_i^{G}(t) + \varepsilon}, \qquad \forall\, i \in \Omega^{g} \tag{5}$$

$$v_i^{T}(t) = V_i^{G}(t) - z_i^{T}(t)\,.\,I_i^{G}(t) \tag{6}$$

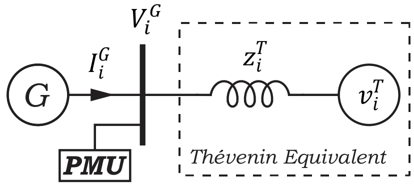

Fig. 3. TEN seen from generator i.

$$\overline{V_i^G}(t+1) = V_i^G(t+1)\,.\,e^{-j\,\Delta\varphi_i(t+1)} \tag{7}$$

$$\overline{I_i^G}(t+1) = I_i^G(t+1)\,.\,e^{-j\,\Delta\varphi_i(t+1)} \tag{8}$$

$$\Delta\varphi_i(t+1) = \Delta\alpha_i(t+1) - \Delta\theta_i(t+1) \tag{9}$$

$$\Delta\alpha_i(t+1) = \alpha_i(t+1) - \alpha_i(t) \tag{10}$$

$$\Delta\theta_i(t+1) = \frac{\pi}{4}\,.\,ROCOF(t+1)\,.\,\lambda^2 \tag{11}$$

where V_i^G and I_i^G are phasor values of the ith generator voltage and phase current, respectively. The overbars represent the modified phasor values in which the effects of phase shift and phase drift are considered via (5)–(11). Ω^g shows a set of generator buses. α_i and $\Delta\alpha_i$ are the phase angle and its difference between two consecutive measured values at node i, respectively. $\Delta\theta_i$ indicates the phase shift at node i in which the rate of change of frequency ($ROCOF$) and width of the time window (λ) between two tandem samples are considered. ε in (5) represents a very small value and is used to avoid infinite values once a generator is out of service.

Fig. 4 shows the Thévenin equivalent impedance (TEI) seen from different generators of the IEEE 10-machine system when a 3-phase fault is applied on bus 16 at 0.1 s and cleared at 0.3 s. The figure shows that the generators express stark contrast in TEI values both in steady-state and during fault. Fig. 5 represents the TEIs seen from generator 7 of the same system for several contingency cases, as an illustrative example. It shows that TEI characteristics are different for different contingencies. Similar behavior was observed for Thévenin equivalent voltages. Based on the above discussion, it can be concluded that the TEN parameters provide easily discriminated features for different system statuses, which might be helpful for transient stability prediction.

III. The Proposed Solution Framework

The proposed solution framework consists of feature extraction, feature selection, and training phases, as described below.

A. *Feature Extraction*

Three groups of features are employed in this study of stability prediction.

1) *Steady-state stability index*

This index measures the stability level of a system in pre-fault condition. A system that is operated close to its stability limits is more prone to instability phenomena in case of a fault compared to a system in which preventive prescriptions are strictly met.

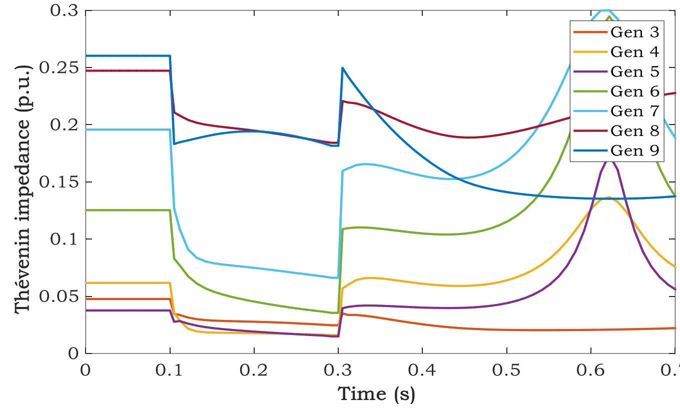

Fig. 4. Thévenin impedance seen from different generators of the 10-machine system with a fault occurring on bus 16 at 0.1 s and cleared at 0.3 s.

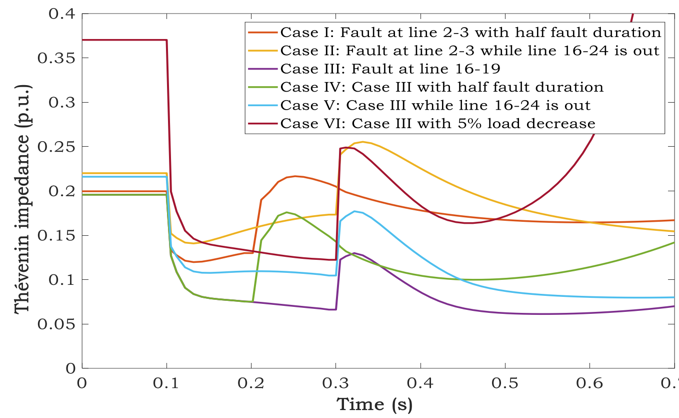

Fig. 5. Thévenin impedance seen from generator 7 of the 10-machine system at different contingencies.

Various indices have been introduced in the literature to assess system status based on rotor angles of generators. Here, the transient stability status at any instant of time is calculated as follows:

$$\psi_i(t) = \frac{\gamma - \overline{\Delta\delta_i}(t)}{\gamma + \overline{\Delta\delta_i}(t)}, \qquad \forall\, i \in \Omega^C \tag{12}$$

$$\overline{\Delta\delta_i}(t) = \max\left(\left|\delta_i^j(t) - \delta_i^k(t)\right|\right), \qquad \forall\, j,k \in \Omega^g \tag{13}$$

where $\delta_i^j(t)$ is the rotor angle of generator j at instant t for contingency i; $\overline{\Delta\delta_i}(t)$ represents the maximum rotor angle deviation between any pair of generators at instant t for contingency i; γ is a cut-off value for rotor angle difference among generators and is set to 2π in this paper; Ω^C and Ω^g show sets of fault contingencies and generator buses, respectively; and $\psi_i(t)$ indicates the stability index of contingency i at instant t, with positive (negative) values indicating a stable (unstable) network.

For a cycle before fault occurring time, t_{F-}, $\psi_i(t_{F-})$ is considered as the steady-state stability index of the system for contingency i and employed as one of the features in the prediction problem.

2) *Fault data related features*

As explained in Section I, event detection algorithms can be used in parallel with stability assessment algorithms. These methods can determine fault type (FT) and fault duration (FD)

by analyzing PMU data. Hence, FT and FD are considered to be features in this study.

3) TEN parameters

Assuming t_{F+} and t_{FC-} are cycles after the fault occurs and before the fault clearing time, respectively, the TEN parameters $(z_i^T(t), v_i^T(t))$ seen from generators at t_{F-}, t_{F+}, and t_{FC-} are considered new features for prediction purposes. Hence, six parameters are calculated for each generator.

B. Feature Selection

The TEN parameters seen from generators at different time frames can provide a huge set of input features for the training process. However, because the number of features is relatively high for large-scale networks, it is vital to apply a feature selection technique to overcome the high dimensionality of the input space and consequently improve the computational efficiency. Moreover, this process can help to reduce the number of generators required for the prediction model and preserve the informative features.

In this paper, a mutual information (MI) based approach, called minimum redundancy-maximum relevancy (mRMR), is employed for feature selection [30]. MI is widely used in the database identification literature and is known as a measure of mutual relevancy of variables. For two variables with observation domains X and Y, it is defined as [30]:

$$MI(X;Y) = \sum_{x\in X}\sum_{y\in Y} p(x,y)\ .\ \log\left(\frac{p(x,y)}{p(x)\ .\ p(y)}\right) \tag{14}$$

where $p(x,y)$ represents the joint probability distribution function (PDF) of X and Y, and $p(x)$ and $p(y)$ respectively denote the PDF of X and Y. x and y indicate any points belonging to X and Y, respectively. Larger values of MI denote that the variables are more correlated.

Assuming C is the desired stability prediction vector resulting from offline analysis, the mRMR first tries to maximize the total relevance of all features (F_i) in subset Ω_{FS}^T of selected features as follows [30]:

$$Max \quad REL(\Omega_{FS}^T, C) \tag{15}$$

$$REL(\Omega_{FS}^T, C) = \frac{1}{|\Omega_{FS}^T|}\ .\ \sum_{F_i\in\Omega_{FS}^T} MI(F_i; C) \tag{16}$$

Then, the redundancy of features with other elements of Ω_{FS}^T is calculated as follows:

$$Min \quad RED(\Omega_{FS}^T) \tag{17}$$

$$RED(\Omega_{FS}^T) = \frac{1}{|\Omega_{FS}^T|^2}\ .\ \sum_{F_i,F_j\in\Omega_{FS}^T} MI(F_i;\ F_j) \tag{18}$$

Finally, the mRMR simultaneously maximizes REL and minimizes RED by (19):

$$\underset{\Omega_{FS}^T\subset\Omega^T}{Max} \ \phi(REL, RED,) \tag{19}$$

$$\phi = REL - RED \tag{20}$$

TABLE II
DATA FOR THE NETWORKS USED IN SIMULATIONS

Network	$\lvert\Omega^b\rvert$	$\lvert\Omega^l\rvert$	# of Transformers	# of Training cases (unstable %)	# of Test cases (unstable %)
10-machine	39	34	12	12000 (28.45%)	3000 (21.77%)
16-machine	68	66	20	15000 (12.81%)	3000 (12.33%)
48-machine	140	206	27	17000 (18.55%)	3000 (18.76%)
50-machine	145	401	52	17000 (15.39%)	3000 (15.83%)

where Ω^T is a set containing all TEN parameters. Once REL and RED are calculated by (16) and (18), a set of TEN parameters selected by the feature selection algorithm (Ω_{FS}^T), through (19), will be used for training purposes, as described next.

C. The Training Process

Based on the proposed approach, a prediction model is found for each FC; the data used for the training process are limited to the area covered by that FC. The features introduced in Section III.A.3 are extracted and the mRMR feature selection method is applied to the training data. The set of Ω_{FS}^T accompanied by the steady-state stability index ($\psi_i(t_{F-})$), FT, and FD, which are introduced in Section II.A, are used as the input features of the prediction engine.

In this paper, ensemble DT is employed to find the optimal classifiers. DT is amongst the most frequently used non-parametric supervised classification techniques [14]. It tries to build a model that predicts the value of a target variable by learning simple decision rules, which are inferred from the data features. An ensemble algorithm consists of a set of classifiers with multiple learning algorithms that find the relation between input features and output target values for different classifiers whose predictions are combined to improve generalizability/robustness over a single classifier [13]. In an ensemble DT, a given database is used to create multiple training sets and a DT-based classifier is developed for each of them. For a new object, each classifier returns its prediction as a vote and the ensemble returns the final decision considering all votes. Several methods have been introduced in the literature to construct DTs and the voting procedure. In this work, the DTs are built with the standard classification and regression tree (CART) and the ensembles are formed based on the boosting technique [13]. Detailed descriptions of DTs and ensemble DTs as well as their application to stability prediction are provided in [13]–[15]; they are not a part of the contribution of this paper and any other tools can be used without loss of generality.

IV. TEST AND RESULTS

To solve the stability prediction problem by the proposed method, the described framework is realized in a MATLAB environment. Several case studies, including IEEE 10-, 16-, 48-, and 50-machine systems, are employed to evaluate the effectiveness of the proposed method. The data required for offline analysis are shown in Table II and generated through the power system toolbox (PST) package [31]. In preparation for the training and test cases, various types of faults are considered; some modifications are implemented in the simulation package based on [32] so that faults can be applied at any point along the transmission lines. The load of each bus is randomly changed between 0.65–

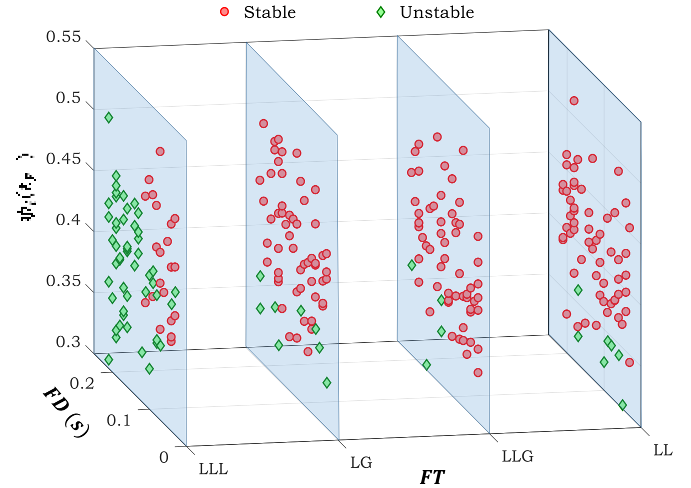

Fig. 6. Distribution of input samples in FT, FD, and $\psi_i(t_{F-})$ plane for an FC representing line 16–17 of the 10–machine system.

TABLE III
SENSITIVITY ANALYSIS OF INPUT FEATURES ON PREDICTION ACCURACY OF THE 10–MACHINE SYSTEM

#	$\psi_i(t_{F-})$	FT, FD	Ω_{FS}^T	Accuracy (%)					
				Training Data			Test Data		
				Stable	Unstable	All	Stable	Unstable	All
1	✓	-	-	97.19	66.37	81.78	93.74	51.3	72.52
2	-	✓	-	95.34	68.36	81.85	94.42	65.08	79.75
3	-	-	✓	99.95	99.84	99.90	98.30	92.34	95.32
4	✓	✓	-	98.21	90.70	94.46	95.82	76.42	86.12
5	✓	-	✓	99.96	99.88	99.92	99.02	94.03	96.53
6	-	✓	✓	99.97	99.80	99.89	99.19	94.95	97.07
7	✓	✓	✓	**100**	**100**	**100**	**99.19**	**95.1**	**97.15**

1.25 of the base value. Moreover, fault duration is randomly selected between 2–15 cycles and fault resistance is arbitrarily chosen based on the lower and upper values reported in [33] for different voltage levels. In addition, offline analysis is conducted so that 85, 14, and 1% of the whole cases are related to nominal power network topology, $N-1$, and $N-2$ contingencies, respectively. Because PST is a frequency-domain simulator, any two consecutive voltage samples are the same in steady-state; so, $z_i^T(t_{F-})$ would be equal to zero for all generators. To resolve this issue, a simple method proposed in [25] is used for TEN calculation during steady-state. All test systems are simulated for 6 s after the fault clearance [14]. Furthermore, PMUs are assumed to provide two measurement samples per cycle [3]. The computer used for the simulations featured an Intel 3.4–GHz CPU with 16 GB of RAM. Two different scenarios are considered in this study, as will be discussed next.

A. *First Scenario*

The first scenario assumes that PMUs are installed in all buses of the network; thus, the number of FCs for each network is equal to the number of transmission lines ($|\Omega^l|$), as shown in Table III. The training process explained in Section III.C is conducted for each FC and the results obtained are reported in Tables III–IV and Figs. 6–9. The classification accuracy for different combinations of input features are shown in Table III for the 10-machine system. The TEN data (Ω_{FS}^T) are able to reach average prediction accuracies of 99.90 and 95.32% for the training and test data, respectively. Moreover, perfect classification accuracy results when all features are employed in the training phase of DTs. Such outcomes not only verify the importance of the TEN parameters proposed in this paper, but also clarify the effectiveness of $\psi_i(t_{F-})$, FT, and FD on overall performance, though each of them alone may not lead to high prediction accuracy. To better illustrate the effects of $\psi_i(t_{F-})$, FT, and FD, distribution of 262 training cases associated with an FC representing faults applied on line 16–17 is shown in Fig. 6. The figure shows that samples with lower $\psi_i(t_{F-})$ are more prone to instability.

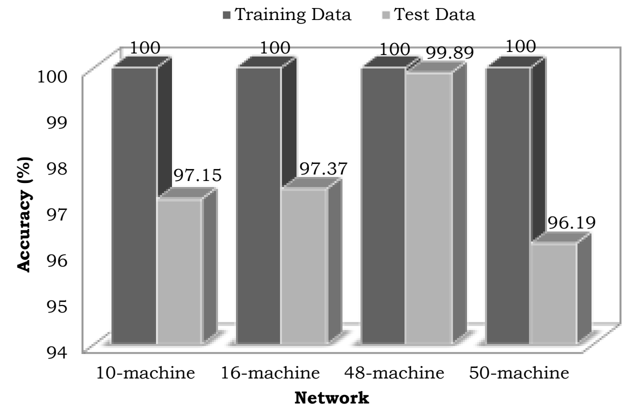

Fig. 7. Performance of the proposed method on training and test data.

TABLE IV
COMPARISON OF RESULTS OF DIFFERENT METHODS FOR STABILITY PREDICTION ON TEST DATA

Method	10-machine	16-machine	48-machine	50-machine
Proposed	**97.15%**	**97.37%**	**99.89%**	**96.19%**
V-PF	95.06%	94.61%	96.25%	94.30%
δ-PF	92.10%	90.27%	91.68%	90.56%
V-DF	95.22%	94.82%	97.36%	94.21%
δ-DF	88.49%	89.53%	90.04%	86.78%

Performance of the proposed framework is compared with state-of-the-art techniques in Table IV. In this table, V-PF and δ-PF respectively represent methods in which 20-cycles of post-fault voltages and rotor angles are used for stability prediction [12], [13]. For the sake of better illustration, in this study both methods are solved with ensemble DT; however, a single model is trained for the whole database as the FC concept is not considered in [12], [13]. Comparing the results obtained for the proposed algorithm with those of V-PF and δ-PF clearly reveals the superior performance of the hybrid FC and Thévenin equivalent-based framework for stability prediction. The classification accuracy of voltage samples are noticebly better than rotor angles, which corroborates the conclusion of [12]. Moreover, the proposed method outperformed other methods in all networks. Notably, V-PF and δ-PF require 20 cycles of post-fault data, which means they respond almost 0.33 s later than the proposed method.

Two extra algorithms, V-DF and δ-DF, are also developed to analyze the effects of TEN parameters in more detail. V-DF and δ-DF respectively stand for an algorithm in which the voltage and rotor angle of generators during fault (at t_{F-}, t_{F+}, t_{FC-}) are used instead of Ω_{FS}^T in the proposed framework. Table IV shows that TEN parameters are more beneficial than voltage samples; this is because TEN parameters contain Thévenin voltages seen from generators, which almost cover the information of bus voltage samples. Detailed information on the proposed classifi-

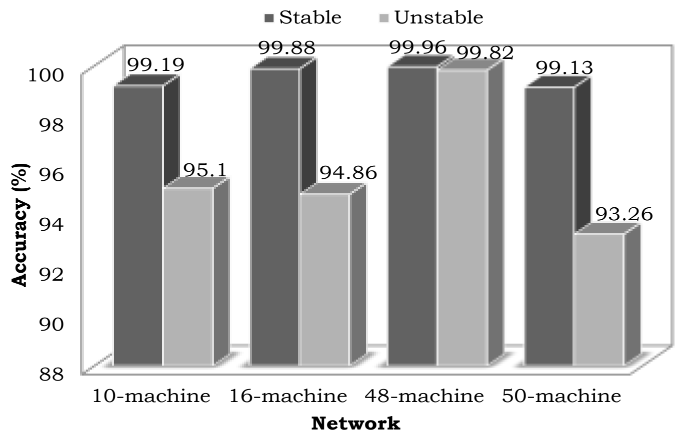

Fig. 8. Performance of the proposed method on test data.

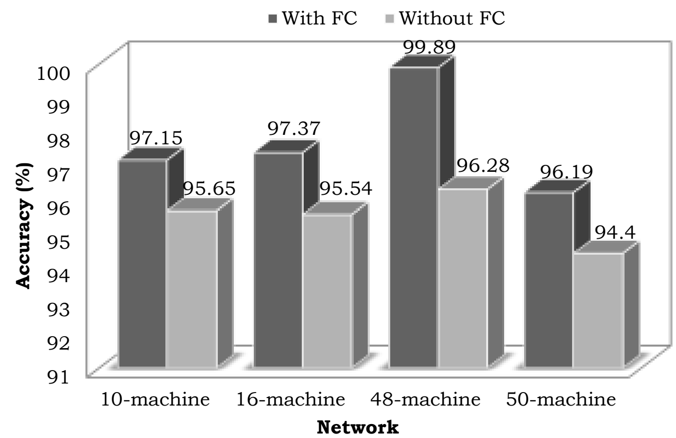

Fig. 9. Performance of the proposed method with/without the FC concept.

TABLE V
SENSITIVITY ANALYSIS OF PMU LOCATIONS WITH COMPLETE OBSERVABILITY ON PREDICTION ACCURACY OF TEST DATA FOR THE 10-MACHINE SYSTEM

Test	Ref.	# of PMUs	PMU locations	# of FCs	Accuracy (%)
1	[34]	8	3, 8, 13, 16, 20, 23, 25, 29	94	98.27
2	[35]	16	8, 10, 16, 18, 24, 26, 28, 30, 31, 32, 33, 34, 35, 36, 37, 38	111	98.60
3	[35]	17	2, 3, 6, 8, 10, 12, 16, 20, 21, 23, 25, 26, 29, 34, 36, 37, 38	54	97.49
4	[35]	18	3, 4, 8, 16, 20, 23, 25, 26, 29, 30, 31, 32, 33, 34, 35, 36, 37, 38	79	97.73
5	--	39	On all buses	34	97.15

TABLE VI
RESULTS OF PREDICTION ACCURACY OF TEST DATA FOR DIFFERENT PMU LOCATIONS WITH INCOMPLETE OBSERVABILITY

Test situation	10-machine	16-machine	48-machine	50-machine
Without PMU noise	97.11%	97.19%	99.35%	95.82%
With PMU noise	95.65%	95.91%	97.82%	94.78%

cations is represented in Fig. 8.

To analyze the effects of the FC concept, the proposed input features in Section III.A are employed to find a single model for the whole training set. The results of this experiment are depicted in Fig. 9, which shows that the FC concept substantially improved the efficacy of the prediction technique; among the studied systems, the 48-machine network experienced the greatest change, with prediction accuracy decreasing from 99.89 to 96.28% if the FCs are ignored.

B. *Second Scenario*

This scenario aims to investigate the performance of the proposed method with respect to various PMU locations and practical issues. Different PMU locations reported in [34], [35] for the 10-machine network are considered in this examination, as shown in Table V. All PMU layouts meet the observability constraint for nominal network topology. Moreover, PMUs in “Test 2”, “Test 3”, and “Test 4” are respectively distributed so that the network remains observable in the case of single line, single PMU, and single line and PMU outages. In addition, PMUs are installed in all buses in “Test 5”, which represents the situation considered in the *First Scenario*. The FCs associated with each PMU layout are calculated based on the procedure explained in Section II.B and a prediction model is trained for each of them. The results obtained for the different analyses are shown in Table V. Because $N-2$ contingences are considered in database generation, both $N-1$ and $N-2$ contingences for lines accompanied by $N-1$ for PMU failures are considered when preparing possible outage sets (Ω^{O}). As can be seen in this Table, 111 FCs are identified for “Test 2”; the FC determination algorithm calculated these FCs in 4.05 s. It is empirically seen in simulations that the maximum FC calculation time for various PMU locations of about 381.77 s belongs to the 50-machine system. Furthermore, the overall training time associated with these FCs was about 869.85 s; considering the parallel nature of the proposed framework, the training time decreased to 13.07 s while running on a 64 processor Intel E5-2660 2.0-GHz CPU with 64 GB of RAM. Table V shows that the prediction accuracy increases from 97.15 to 98.60% by increasing the number of FCs from 34 to 111. However, increasing the number of PMUs, while the system is observable, does not necessarily lead to more FCs and consequently better classification accuracy. For instance, the lowest accuracy in Table V is related to a situation in which PMUs are installed in all buses (“Test 5”). In comparison with “Test 1” in which 94 FCs are required, the FCs in “Test 5” cannot provide any extra information about the system configuration as they remain unchanged for all discussed contingencies (such as line failures).

To evaluate the effects of PMU layout with incomplete observability, PMU locations are calculated based on [28]. Three different PMU locations are generated for each network and the stability prediction problem is repeated. Average classification accuracies are reported in Table VI. The results are very close to those of Table IV and show that the proposed framework can bring about satisfactory results with different numbers of PMUs.

The performance of the proposed method is also investigated in the presence of PMU noise. To this end, all offline data are randomly changed by ±2% and the training process is repeated [9]. The results are illustrated in Table VI. Compared to the situation in which PMU noise is ignored, the average prediction accuracy of all networks decreases by 1.33%. Based on the IEEE C37.118.1-2011 standard, the total vector error of the phasor measured by PMU should be less than 1%; hence, the proposed method can perform better in real-life situations compared to this overly harsh analysis.

V. Conclusion

This paper proposed a novel solution approach for transient stability prediction. The framework introduced, which is inspired by PMU related studies, employs an FC concept to find multiple prediction models for an interconnected power system. Feature extraction is conducted by obtaining TEN parameters at different instances of time in both steady-state and during fault. In addition, a feature selection algorithm is applied to decipher the most discriminative features as inputs of the training engine. The method developed was successfully tested on several IEEE test systems; the results obtained and comparisons reported show that the proposed approach is an effective tool for transient stability prediction of power systems.

Further research could be conducted to enhance the performance of the proposed method through different machine learning techniques. Moreover, because the introduced framework does not require post-fault data, its prediction might be used as an input feature for a wide array of stability prediction methods reported in the literature.

References

[1] P. Kundur, *et al.*, “Definition and classification of power system stability IEEE/CIGRE joint task force on stability terms and definitions,” *IEEE Trans. Power Syst.*, vol. 19, no. 3, pp. 1387–1401, 2004.

[2] E. Vaahedi, *Practical Power System Operation*, Piscataway, NJ: Wiley, 2014.

[3] S. Dasgupta, M. Paramasivam, U. Vaidya, and V. Ajjarapu, “PMU-based model-free approach for real-time rotor angle monitoring,” *IEEE Trans. Power Syst.*, vol. 30, no. 5, pp. 2818–2819, 2015.

[4] M.A. Tomim, J.R. Martí, and J.A.P. Filho, “Parallel transient stability simulation based on multi-area Thévenin equivalents,” *IEEE Trans. Smart Grid*, vol. 8, no. 3, pp. 1366–1377, 2017.

[5] C. Wang, K. Yuan, P. LI, B. Jiao, and G. Song, “A projective integration method for transient stability assessment of power systems with a high penetration of distributed generation,” *IEEE Trans. Smart Grid*, vol. PP, no. 99, pp. 1–10, 2017.

[6] M. Oluic, M. Ghandhari, and B. Berggren, “Methodology for rotor angle transient stability assessment in parameter space,” *IEEE Trans. Power Syst.*, vol. 32, no. 2, pp. 1202–1211, 2017.

[7] P. Bhui and N. Senroy, “Real-time prediction and control of transient stability using transient energy function,” *IEEE Trans. Power Syst.*, vol. 32, no. 2, pp. 923–934, 2017.

[8] T.L. Vu and K. Turitsyn, “Lyapunov functions family approach to transient stability assessment,” *IEEE Trans. Power Syst.*, vol. 31, no. 2, pp. 1269–1277, 2016.

[9] J.J.Q. Yu, D.J. Hill, A.Y.S. Lam, J. Gu, and V.O.K. Li, “Intelligent time-adaptive transient stability assessment system,” *IEEE Trans. Power Syst.*, vol. pp, no. 99, pp. 1–10, 2017.

[10] N. Amjady and S.A. Banihashemi, “Transient stability prediction of power systems by a new synchronism status index and hybrid classifier,” *IET Gener. Transm. Dis.*, vol. 4, no. 4, pp. 509–518, 2010.

[11] A.N. AL-Masri, M.Z.A Kadir, H. Hizam, and N. Mariun, “A novel implementation for generator rotor angle stability prediction using an adaptive artificial neural network application for dynamic security assessment,” *IEEE Trans. Power Syst.*, vol. 28, no. 3, pp. 2516–2525, 2013.

[12] F.R. Gomez, A.D. Rajapakse, U.D. Annakkage, and I.T. Fernando, “Support vector machine-based algorithm for post-fault transient stability status prediction using synchronized measurements,” *IEEE Trans. Power Syst.*, vol. 26, no. 3, pp. 1474–1483, 2011.

[13] T. Guo and J.V. Milanovic, “Online identification of power system dynamic signature using PMU measurements and data mining,” *IEEE Trans. Power Syst.*, vol. 31, no. 3, pp. 1760–1768, 2016.

[14] T. Amraee and S. Ranjbar, “Transient instability prediction using decision tree technique,” *IEEE Trans. Power Syst.*, vol. 28, no. 3, pp. 3028–3037, 2013.

[15] H. Supreme, L.A. Dessaint, I. Kamwa, and A. Heniche-Oussedik, “Development of new predictors based on the concept of center of power for transient and dynamic instability detection,” *IEEE Trans. Smart Grid*, vol. pp, no. 99, pp. 1–11, 2017.

[16] B. Wang, B. Fang, Y. Wang, H. Liu, and Y. Liu, “Power system transient stability assessment based on big data and the core vector machine,” *IEEE Trans. Smart Grid*, vol. 7, no. 5, pp. 2561–2570, 2016.

[17] R. Zhang, Y. Xu, Z.Y. Dong, and K.P. Wong, “Post-disturbance transient stability assessment of power systems by a self-adaptive intelligent system,” *IET Gener. Transm. Dis.*, vol. 19, no. 5, pp. 296–305, 2015.

[18] Q. Jiang, X. Li, B. Wang, and H. Wang, “PMU-based fault location using voltage measurements in large transmission networks,” *IEEE Trans. Power Del.*, vol. 27, no. 3, pp. 1644–1652, 2012.

[19] J.W. Lee, W.K Kim, J. Han, and W.H. Jang, C.H Kim, “Fault area estimation using traveling wave for wide area protection,” *J. Mod. Power Syst. Clean Energy*, vol. 4, no. 3, pp. 478–486, 2016.

[20] J. Ma, J.L Li, Z.P. Wang, and Q.X. Yang, “A novel wide-area fault location algorithm based on fault model,” in *Proc. Power and Energy Engineering Conf.*, pp. 1-4, 2010.

[21] P. Bhui and N. Senroy, “Online identification of tripped line for transient stability assessment,” *IEEE Trans. Power Syst.*, vol. 31, no. 3, pp. 2214–2224, 2016.

[22] Y. Ge, A.J. Flueck, D.K. Kim, and J.B. Ahn, J.D. Lee, D.Y Kwon, “Power system real-time event detection and associated data archival reduction based on synchrophasors,” *IEEE Trans. Smart Grid*, vol. 6, no. 4, pp. 2088–2097, 2015.

[23] B. Alinezhad and H.K. Karegar, “On-line Thévenin impedance estimation based on PMU data and phase drift correction,” *IEEE Trans. Smart Grid*, vol. pp, no. 99, pp. 1–9, 2016.

[24] S.M. Abdelkader and D.J. Morrow, “Online Thévenin equivalent determination considering system side changes and measurement errors,” *IEEE Trans. Power Syst.*, vol. 30, no. 5, pp. 2716–2725, 2015.

[25] B. Alinezhad and H.K. Karegar, “Online inertia constant and Thévenin equivalent estimation using PMU data,” *Int. J. Smart Elec. Eng.*, vol. 3, no. 3, pp. 73–78, 2014.

[26] G. Ravikumar and S.A. Khaparde, “Taxonomy of PMU data based catastrophic indicators for power system stability assessment,” *IEEE Syst. J.*, vol. PP, no. 99, pp. 1–13, 2016.

[27] F. Aminifar, *et al.*, “Synchrophasor measurement technology in power systems: Panorama and state-of-the-art,” *IEEE Access*, vol. 2, no. 1, pp. 1607–1628, 2014.

[28] R.F. Nuqui and A.G. Phadke, “Phasor measurement unit placement techniques for complete and incomplete observability,” *IEEE Trans. Power Del.*, vol. 20, no. 4, pp. 2381–2388, 2005.

[29] J. Yi, T. Clausen, and U. Herberg, “Depth-first forwarding for unreliable networks: Extensions and applications,” *IEEE Internet Things J.*, vol. 2, no. 3, pp. 199–209, 2015.

[30] W.X. Wang, Y.C. Lai, and C. Grebogi, “Data based identification and prediction of nonlinear and complex dynamical systems,” *Physics Reports*, Vol. 664, no. 1, pp. 1–76, 2016.

[31] J.H. Chow and K.W. Cheung, “A toolbox for power system dynamics and control engineering education and research,” *IEEE Trans. on Power Syst.*, vol.7, no.4, pp.1559-1564, Nov 1992

[32] J. Arrillaga and N.R. Watson, *Computer modelling of electrical power systems*. 2nd ed. Chichester, UK: Wiley, 2001.

[33] V. D. Andrade and E. Sorrentino, “Typical expected values of the fault resistance in power systems,” in *Proc. IEEE/PES Transmiss., Distrib. Conf. Expo.*, Nov. 8–10, 2010, pp. 602–609.

[34] M. Rashidi and E. Farjah, “Lyapunov exponent-based optimal PMU placement approach with application to transient stability assessment,” *IET Sci., Meas. & Tech.*, vol. 10, no. 5, pp. 492–497, 2016.

[35] K.G. Khajeh, E. Bashar, A.M. Rad, and G.B. Gharehpetian, “Integrated model considering effects of zero injection buses and conventional measurements on optimal PMU placement,” *IEEE Trans. Smart Grid*, vol. 8, no. 2, pp. 1006–1013, 2017.